Supplement of Atmos. Chem. Phys., 23, 4741–4761, 2023
https://doi.org/10.5194/acp-23-4741-2023-supplement

Atmospheric Chemistry and Physics
Open Access
EGU

Supplement of

Ice-nucleating particles in northern Greenland: annual cycles, biological contribution and parameterizations

Kevin C. H. Sze et al.

Correspondence to: Heike Wex (wex@tropos.de) and Frank Stratmann (stratmann@tropos.de)

S1 Sample summary and merging procedure of INP spectra from LINA and INDA

Table S1. Summary of the amount of filters analyzed. In total 181 filter samples were presented in this study.

Month	**Year**			**Sum**
	2018	2019	2020	
January	–	7	6	13
February	–	8	8	16
March	–	7	7	14
April	–	9	8	17
May	–	7	8	15
June	–	7	9	16
July	4	7	9	20
August	1	3	9	13
September	8	6	4	18
October	8	9	–	17
November	7	5	–	12
December	1	9	–	10

As mentioned in the main text, all spectra of untreated samples shown in this study are merged from the individual LINA and INDA spectra of the respective sample. The procedure to achieve the merged spectra is described in the following paragraphs. The first two steps of the merging procedure are associated with data quality assurance: Due to the temperature calibration functions for LINA and INDA, the temperatures at which the f_{ice}(T) were measured differ for the two setups. Details on the calibration of LINA and INDA can be found in the SI of Hartmann et al. (2021). To obtain unified temperatures for all data sets, in a first step, a linear interpolation was done for all measured frozen fraction spectra of LINA and INDA. This resulted in f_{ice}(T) for every tenth of a degree. As the second step of the merging procedure, the spectra of LINA and INDA were truncated, i.e., f_{ice}(T) corresponding to the first three and last two frozen droplets were deleted, i.e. for LINA, $\frac{3}{90} < f_{ice}(T) < \frac{89}{90}$; while for INDA, $\frac{3}{48} < f_{ice}(T) \leq \frac{46}{48}$. This was done due to the large statistical uncertainty of this data. As the next step of the merging procedure, the area between the LINA and INDA spectra in the overlap temperature range was quantified as the sum of the absolute difference of INP number concentration (per volume of water) $N_{INP,water}$ at each temperature, divided by the temperature range of the overlap region. An example is shown in Fig. S1a. Those spectra that had an area larger than the 95^{th} percentile of the whole data-set were discarded from further analysis. The remaining spectra fulfilled the authors' standards for data quality and were then converted into atmospheric INP number concentration $N_{INP,air}$ (see Fig. S1b) and merged as described as follows: A merging weighting factor F(T) was calculated for both LINA and INDA spectra based on their corresponding frozen fraction. The idea behind F(T) is to account for the fact that a high f_{ice} value, and the N_{INP} value derived from it, is statistically more certain than a low one. When the spectra are merged, the statistically more certain values at a given T should therefore be weighted more strongly. F(T) is calculated as follows:

$$F_{\mathrm{LINA}}(T) = \frac{f_{\mathrm{ice,LINA}}(T)}{f_{\mathrm{ice,LINA}}(T) + f_{\mathrm{ice,INDA}}(T)} \tag{1}$$

and

$$F_{\mathrm{INDA}}(T) = \frac{f_{\mathrm{ice,INDA}}(T)}{f_{\mathrm{ice,LINA}}(T) + f_{\mathrm{ice,INDA}}(T)} \tag{2}$$

By using the merging weighting factors above, the INP number concentration of the merged spectrum ($N_{INP,merge}$) in the overlap region is then calculated as

$$N_{\mathrm{INP,merge}}(T) = N_{\mathrm{INP,LINA}}(T) \cdot F_{\mathrm{LINA}}(T) + N_{\mathrm{INP,INDA}}(T) \cdot F_{\mathrm{INDA}}(T) \tag{3}$$

where $N_{INP,LINA}(T)$ is the INP number concentration of LINA spectra in the overlap region, while $N_{INP,INDA}(T)$ is the INP number concentration of INDA spectra in the overlap region. Along with the non-overlap region, a full INP spectrum (i.e. merged region, non-overlap INDA region, non-overlap LINA region) is derived (see Fig. S1c). For simplicity, the atmospheric INP number concentration of the full spectrum is denoted as N_{INP} in this study. It is also worth to point out that by merging INP spectra of LINA and INDA, it is possible that in rare cases, as temperature decreases, the INP number concentration of the full spectrum decreases.

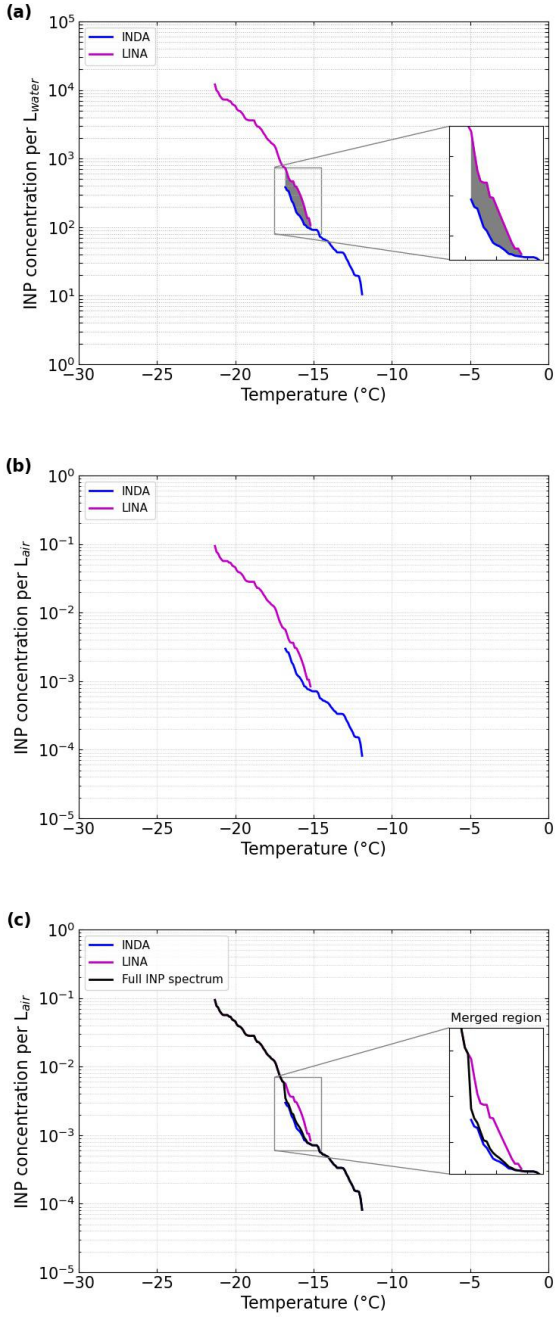

Figure S1. A schematic sketch of the merging procedures performed in this study. a) After interpolation and truncation of both LINA (in purple) and INDA (in blue) spectra, the consistency of the spectra was evaluated by quantifying the area (gray color) between the two spectra. Note that the INP concentration shown here is per liter of water. Spectra showed area large than 95^{th} percentile of the whole data-set were discarded. b) INP concentration per liter of air of the remaining samples was calculated. c) Merging was taken place followed the calculations mentioned in text. The INP concentration N_{INP} of the full spectrum (in black) was then used for data interpretation.

S2 Blank filter measurements

Fig. S2 exemplarily shows measured frozen fractions ($f_{ice}(T)$) for blank filters and respective atmospheric samples. Data are given for both measurement devices LINA and INDA (see main text for more details), and for all samples collected in the months of February and July. Data are shown separately for the two months, as blank filter values are generally higher in summer than in winter, an observation which was made before (Wex et al., 2019). Even within July, blank filters with the highest values correspond to atmospheric samples with higher concentrations.

The blank filter values were clearly below the values from the atmospheric samples. It also can be seen that the temperature range covered by the data from the blank filters is at lower temperatures than that of the measurements. Therefore, correcting the measurements with background data would only be partially possible. Also, a correction is done based on concentrations (Vali, 2019), i.e., using the logarithms of $f_{ice}(T)$, such that corrections for the data used in this study are small and no influence on the outcome of our overall results is observed. Therefore, a background subtraction was not done.

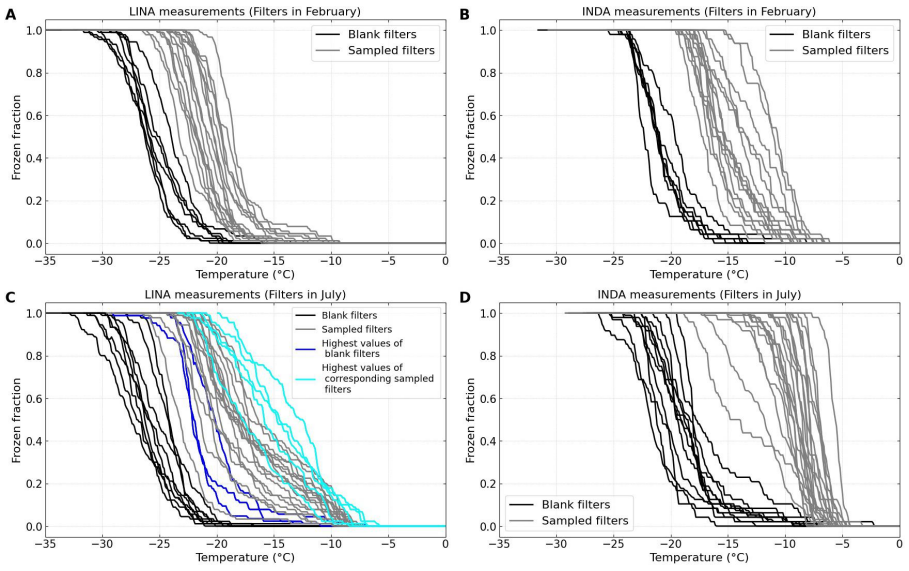

Figure S2. Measured $f_{ice}(T)$ for blank filters and respective atmospheric samples for LINA (left panels) and INDA (right panels), showing all samples for the month of February (upper panels) and July (lower panels). Blank filter data are always shown in black, atmospheric sample data in gray, except for LINA data for July (panel C, lower left side), for which data for the blank filters with the highest values are given in blue and the corresponding filters in cyan.

S3 Instrumental uncertainties of LINA and INDA

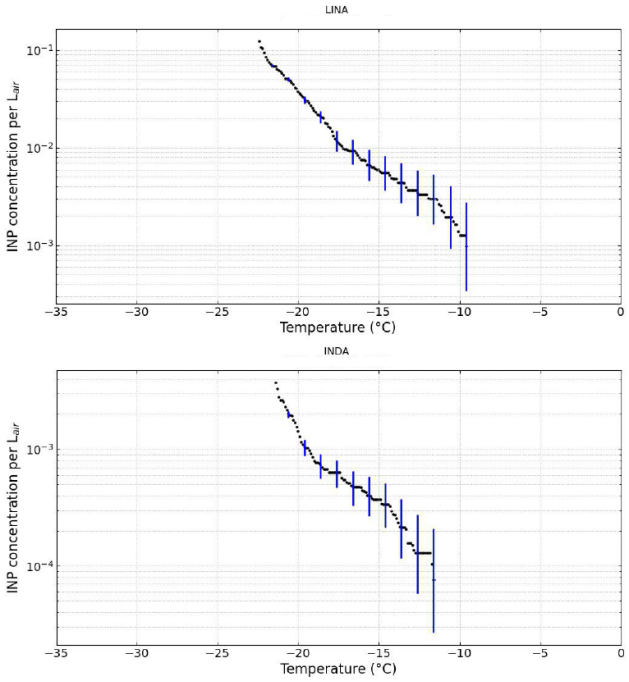

Figure S3. Example of INP spectra from two different filters with error bars in blue color showing the instrumental uncertainties of LINA (upper panel) and INDA (lower panel) in every 1°C step.

S4 Overview of INP spectra obtained in different years

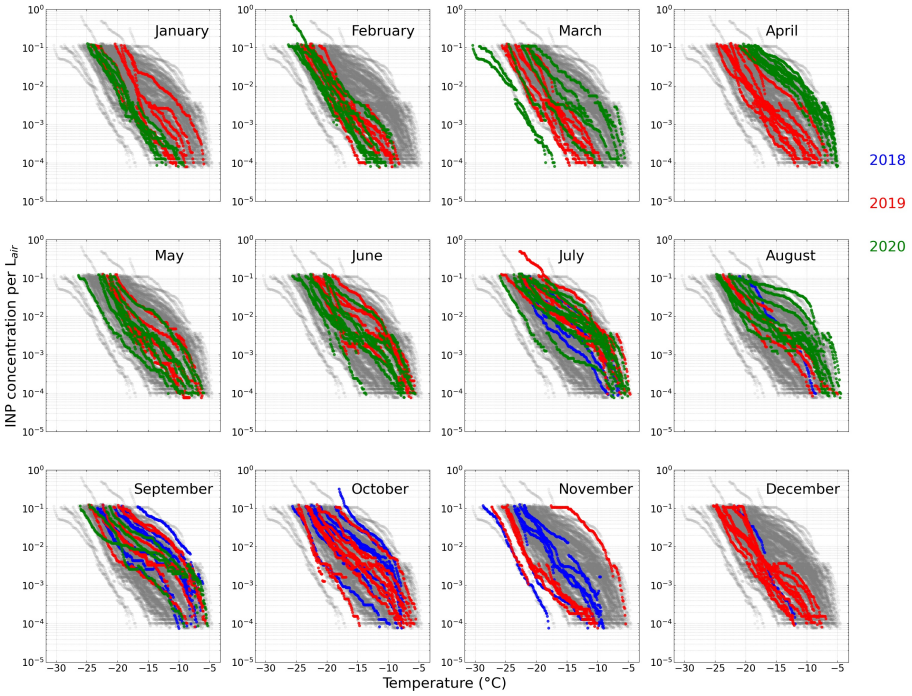

Figure S4. An overview of all INP spectra obtained in this study, color-coded by their corresponding year. Blue color shows samples collected in 2018, red color shows samples collected in 2019, green color shows samples collected in 2020, grey color shows all samples regardless of the collection months.

S5 Snow depth at Villum Research Station

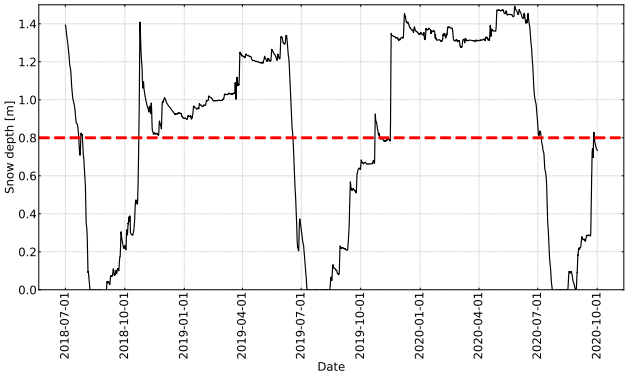

Figure S5. Snow depth measured at Villum Research Station from July 2018 to September 2020.

S6 Overview of INP spectra obtained for different types

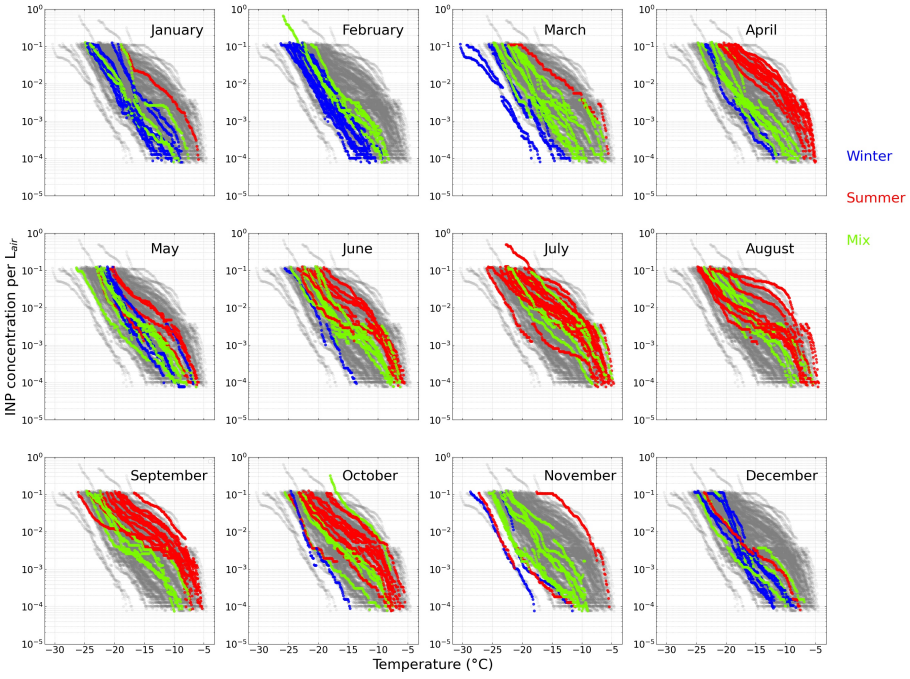

Figure S6. Similar figure as Fig. S4, color-coded by the types of categorization. Blue color shows samples characterized as winter type, red color shows samples characterized as summer type, light green shows samples characterized as mix type, while grey color shows all samples regardless of their type.

Table S2. Summary of the amount of filters characterized as winter, mix and summer type.

Month	**Year**								
	2018			2019			2020		
	Winter	Mix	Summer	Winter	Mix	Summer	Winter	Mix	Summer
January	–	–	–	5	1	1	4	2	0
February	–	–	–	4	4	0	6	2	0
March	–	–	–	3	4	0	2	4	1
April	–	–	–	2	6	1	0	0	8
May	–	–	–	3	2	2	2	4	2
June	–	–	–	0	3	4	1	5	3
July	0	2	2	0	1	6	0	2	7
August	0	1	0	0	2	1	0	2	7
September	0	2	6	0	2	4	0	1	3
October	0	4	4	1	2	6	–	–	–
November	2	5	0	0	3	2	–	–	–
December	1	0	0	5	3	1	–	–	–

S7 Arctic INP parameterization

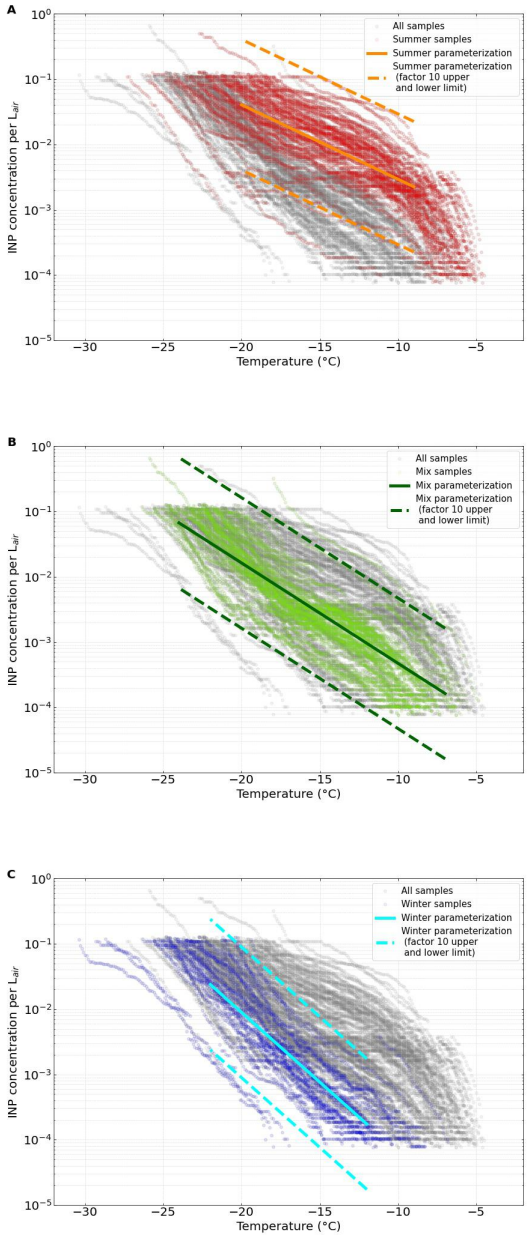

Figure S7. Each panel shows all INP spectra in gray color in the background of all panels, as reference. Additionally, all summer, mix and winter type spectra are shown in red, green and blue in panel A, B and C, respectively. Also shown are the suggested respective parameterizations (solid lines) and a deviation from them by a factor of 10 (dashed lines).

S8 Heat-labile ratio in connection to INP spectra characterization

In a further step, the fraction of heat-labile INPs, i.e., the heat-labile ratio (see Section 3.4 in the main text), in relation to the classification described in Section 3.2 in the main text was also investigated. The result is shown in Fig. S8. Indeed, at the depicted temperatures, for winter type samples, there are low heat-labile ratios of mostly only up to 50%, while summer type samples show high heat-labile ratios of mostly above 75%. The mix type samples are in between. This once more corroborates that the selected simple criteria to discriminate between the three different types of INP spectra are also in accordance with other INP properties which change over the year.

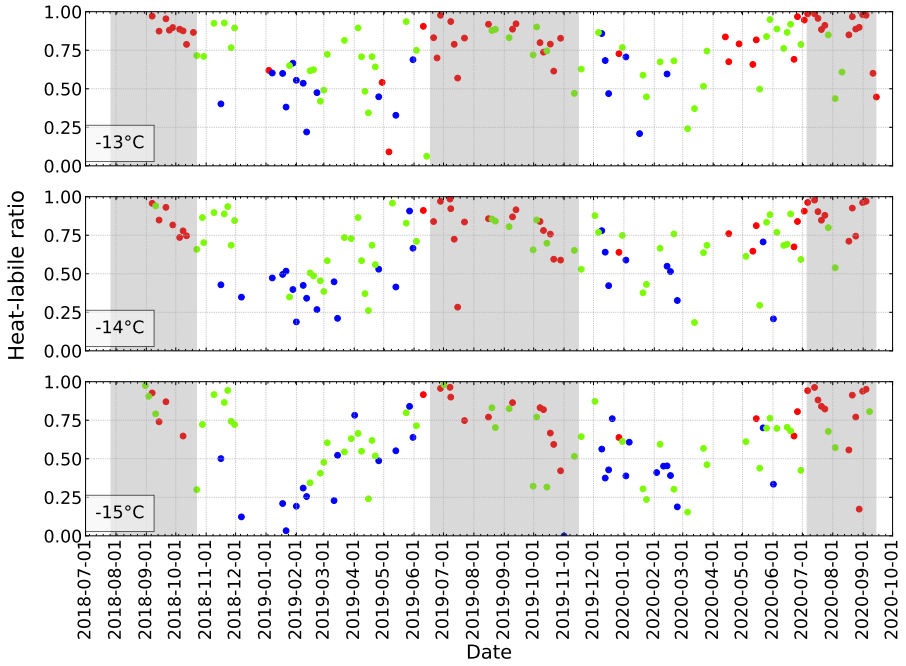

Figure S8. Time series of fractions of heat-labile INPs at three different temperatures, -13°C, -14°C and -15°C, with winter type data shown in blue, summer type data shown in red and mix type data shown in light green.

S9 Case study

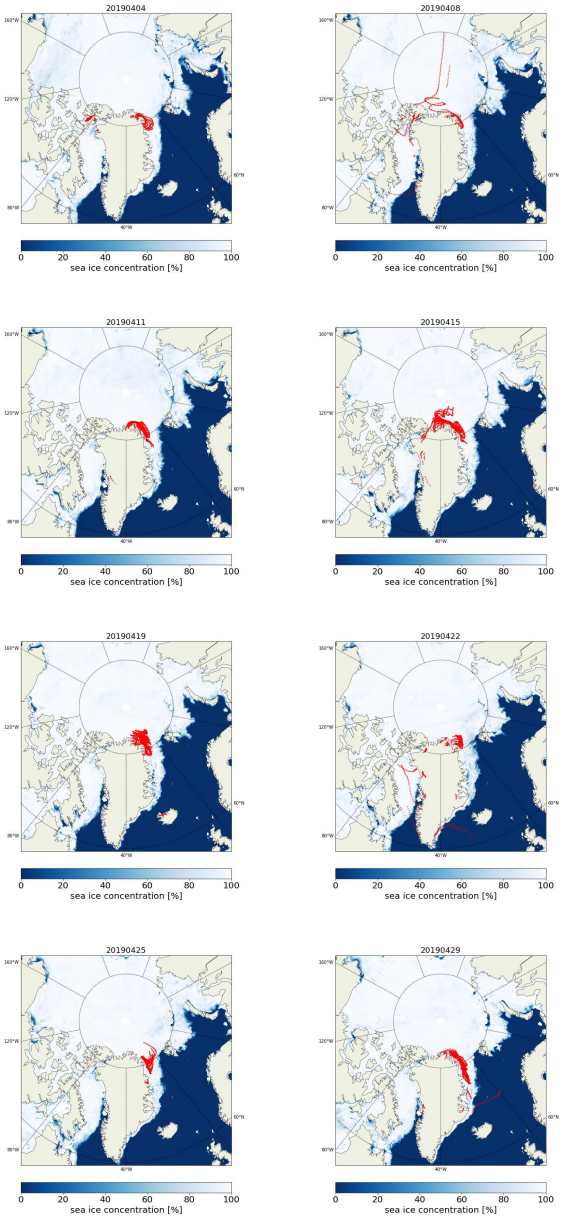

Figure S9. Each map shows trajectories and sea ice concentrations corresponding to an individual filter sample. All filters collected in April 2019 are shown. The sampling end date of the filters is shown on top of the maps. 5-day back-trajectories (arriving at VRS at a height of 50m) are indicated in red for locations where they were below 250m height. Average sea ice concentrations for the respective sampling periods are also shown.

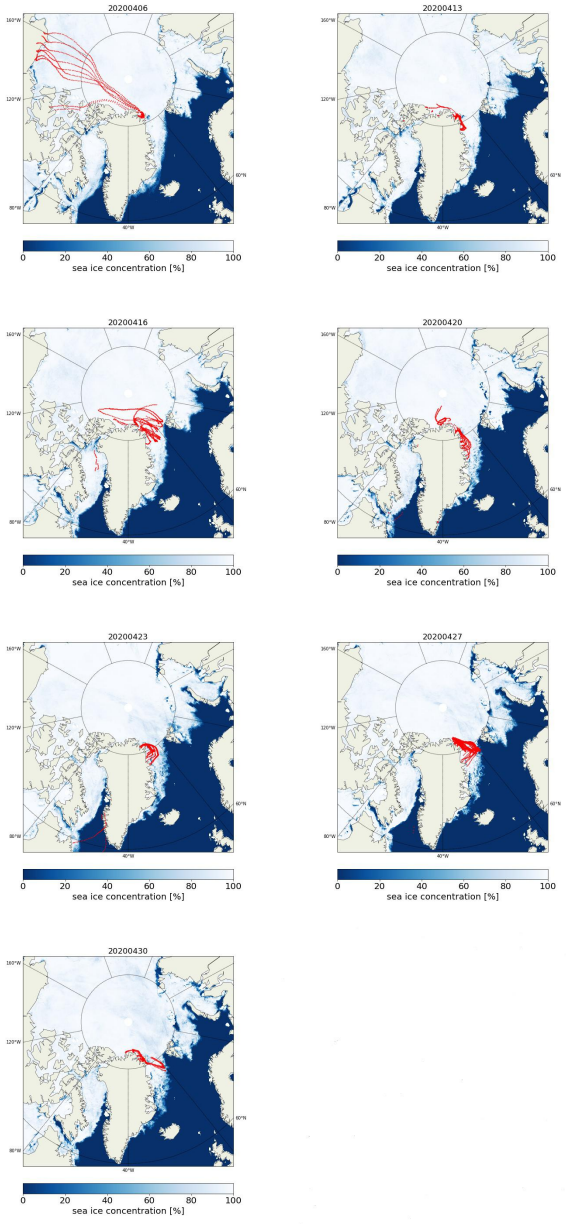

Figure S10. Each map shows trajectories and sea ice concentrations corresponding to an individual filter sample. All filters collected in April 2020 are shown. The sampling end date of the filters is shown on top of the maps. 5-day back-trajectories (arriving at VRS at a height of 50m) are indicated in red for locations where they were below 250m height. Average sea ice concentrations for the respective sampling periods are also shown.

Table S3. Summary of the frequency of surface types shown in Fig. 10(a) in the main text. Values are expressed in %.

Surface type	**Date**								
	20190401	20190404	20190408	20190411	20190415	20190419	20190422	20190425	20190429
terrestrial	48.47	48.35	39.36	27.70	18.23	10.74	41.10	21.12	16.41
ice (90-100%)	47.65	45.19	49.86	65.29	78.85	86.71	45.13	55.45	74.82
ice (75-90%)	1.12	5.67	6.49	6.50	2.53	1.84	7.08	17.13	5.34
ice (50-75%)	0.82	0.66	2.21	0.42	0.34	0.42	1.47	4.90	1.18
ice (below 50%)	1.43	0.13	1.10	0.08	0.05	0.09	0.49	1.40	0.69
sea	0.51	0	0.97	0	0	0.19	4.72	0	1.57

Table S4. Summary of the frequency of surface types shown in Fig. 10(b) in the main text. Values are expressed in %.

Surface type	**Date**							
	20200406	20200410	20200413	20200416	20200420	20200423	20200427	20200430
terrestrial	16.86	66.35	46.55	7.81	25.90	28.44	15.66	27.5
ice (90-100%)	70.32	26.09	50.96	89.06	65.04	25.74	45.67	51.92
ice (75-90%)	12.13	5.67	2.49	2.73	5.90	20.72	18.95	12.88
ice (50-75%)	0.69	1.51	0	0.20	1.58	9.14	10.12	4.42
ice (below 50%)	0	0.38	0	0.20	0.58	7.98	8.77	2.5
sea	0	0	0	0	1.01	7.98	0.82	0.77

Figure S11. Correlation plot between N_{INP} at -12°C and -18°C and all examined meteorological parameters in April 2019. Value R shows the Spearman coefficient.

Figure S12. Correlation plot between N_{INP} at -12°C and -18°C and all examined meteorological parameters in April 2020. Value R shows the Spearman coefficient.

References

Hartmann, M., Gong, X., Kecorius, S., van Pinxteren, M., Vogl, T., Welti, A., Wex, H., Zeppenfeld, S., Herrmann, H., Wiedensohler, A., and Stratmann, F.: Terrestrial or marine – indications towards the origin of ice-nucleating particles during melt season in the European Arctic up to 83.7° N, Atmospheric Chemistry and Physics, 21, 11 613–11 636, https://doi.org/10.5194/acp-21-11613-2021, 2021.

Vali, G.: Revisiting the differential freezing nucleus spectra derived from drop-freezing experiments: methods of calculation, applications, and confidence limits, Atmospheric Measurement Techniques, 12, 1219–1231, https://doi.org/10.5194/amt-12-1219-2019, 2019.

Wex, H., Huang, L., Zhang, W., Hung, H., Traversi, R., Becagli, S., Sheesley, R. J., Moffett, C. E., Barrett, T. E., Bossi, R., Skov, H., Hünerbein, A., Lubitz, J., Löffler, M., Linke, O., Hartmann, M., Herenz, P., and Stratmann, F.: Annual variability of ice-nucleating particle concentrations at different Arctic locations, Atmospheric Chemistry and Physics, 19, 5293–5311, https://doi.org/10.5194/acp-19-5293-2019, 2019.